Design and Analysis of High-Resolution Electrostatic Adhesive Brakes Towards Static Refreshable 2.5D Tactile Shape Display

Kai Zhang, *Student Member, IEEE*, Eric J. Gonzalez, *Student Member, IEEE*, Jianglong Guo, and Sean Follmer, *Member, IEEE*

***Abstract*—Tactile displays are haptic devices capable of rendering shape and texture information. Unsolved challenges in building tactile shape displays include their traditionally large form factors, low spatial resolution, and high costs. Using electrostatic adhesion to individually brake each pin and a single platform for global actuation, we developed a prototype static refreshable tactile shape display with high spatial resolution (1.7 mm pitch, 0.8 mm pin width; 4 mm pitch, 1.6 mm pin width), high resistance force (76.3 gf static-loading force per pin for 1.6 mm width) and low cost ($0.11 USD per pin for raw material). We present an analytical model of our electroadhesive brake mechanism and evaluate its maximum contact force and robustness in various conditions. To demonstrate the mechanism's potential, we built a static tactile shape display prototype with a 4×2 array of pins controlled using electroadhesive brakes. To further increase maximsum contact force allowed by our device, we develop and evaluate a global mechanical clutch which can be engaged during user interaction. A user study is carried out to compare our static tactile shape display's performance with printed 2.5D tactile graphics in a shape recognition task, and comparable shape recognition rates and response times are observed.**

***Index Terms*—Electrostatic adhesive brake, tactile display, shape display, encountered-type haptics.**

I. Introduction

TACTILE displays enable users to perceive small-scale surface and shape characteristics with their fingers and hands. Unlike audiovisual feedback, tactile output affords richer physical interactions and leverages the innate dexterity and spatial acuity of our hands and fingers. Tactile displays have been explored in applications for improving information accessibility of visual-impaired people [1]–[3], telepresence [4]–[7], and human-computer interaction (HCI) [8], [9]. Most commonly these displays are achieved through actuating an array of tactors, or pins, which can be raised or lowered to create rasterized shapes and surfaces. Among tactile displays, 2.5D tactile displays distinguish themselves by enabling larger pin displacements, allowing them to render larger-scale 2.5D approximations of an object's global shape, similar to a relief sculpture. An advantage of large 2.5D tactile arrays is that they afford whole hand interaction, which is important for gross shape perception especially in the context of tactile graphics for blind and visually impaired people. And while other researchers have achieved promising results with a variety of techniques, including creating illusions of shape perception using a simple tilting platform to display the first order information of a curved surface [10], [11], these approaches cannot support such interaction.

Tactile displays can usually be categorized into static refreshable displays and dynamic displays [3]. Static refreshable displays, while they are unable to provide interactive haptic feedback at rates commonly found in traditional haptic interfaces, have many potential uses especially in the context of tactile spatial graphics for people who are blind or visually impaired, where it may take significant time to fully explore a shape. An ideal static refreshable 2.5D tactile shape display should possess high spatial resolution for shape recognition ($\approx$ 2-3 mm [12]), sufficient refresh rate ($\approx$ 10 second [3]) and support contact forces of at least 50 gf generated by the user's finger during feature exploration [13]. Cost is another important consideration: if manufacturing costs (e.g., raw material, assembling and testing) can be reduced for a large scale (100×100) high-resolution shape display to less than $0.10 USD per pin, it will be available at a price comparable to other consumer electronics device (e.g., a smartphone or laptop). The device should also be lightweight and enable large pin displacements to support a wide variety of tactile rendering scenarios.

Various actuation techniques have been explored for dynamic and static 2.5D tactile displays including linear actuators [6], [8], [14], [15], electromagnetic (EM) actuation [16], shape-memory alloys (SMA) [17], [18], hydraulic actuation [19], microelectromechanical systems (MEMS) [20] and piezoelectric actuation [21], [22] (see [3] or [7] for a comprehensive review). These actuation techniques have several trade-offs.

Manuscript received December 14, 2018; revised August 19, 2019; accepted August 24, 2019. Date of publication September 19, 2019; date of current version December 12, 2019. This paper was recommended for publication by Associate Editor F. Giraud upon evaluation of the reviewers' comments. This work was supported by the Stanford Graduate Fellowship. *(Corresponding author: Kai Zhang.)*

K. Zhang, E. J. Gonzalez, and S. Follmer are with the Department of Mechanical Engineering, Stanford University, Stanford, CA 94305, USA (e-mail: kzhang3@stanford.edu; ejgonz@stanford.edu; sfollmer@stanford.edu).

J. Guo is with the SoftLab, University of Bristol, BS8 1TH Bristol, U.K. (e-mail: j.guo@bristol.ac.uk).

This paper has supplementary downloadable material available at http://ieeexplore.ieee.org, provided by the authors.

Digital Object Identifier 10.1109/TOH.2019.2940219

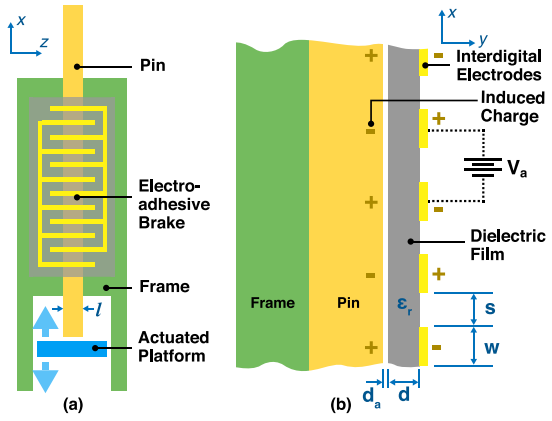

Fig. 1. Diagram (a) and cross-section (b) of an individual electrostatic adhesive brake. Electrostatic attraction is generated between the interdigital electrodes and the brass pin when a voltage differential is applied.

Mechanical linear actuator-based tactile displays provide large contact force but are generally bulky and expensive due to the cost of many linear actuators in the system. Electromagnetic (EM) actuation methods often suffer from low force capacity and magnetic interference issues, and thus are not very stable. Shape-memory alloy (SMA)-based tactile displays utilize thermal expansion to control individual pins; however, high current requirements significantly increase power consumption. Jungmann and Schlaak [23] proposed a tactile display using electrostatic actuation of elastic dielectric elements. This method enables low cost and lightweight actuation, but only supports small pin displacements.

Compared to the more common actuator-per-pin paradigm of tactile displays (used in dynamic displays), a brake-per-pin approach has some distinct advantages. Namely, brake-based displays can be made more compact and potentially much lower cost since hundreds of actuators are not needed; instead, a single actuator acts to globally raise and lower all pins at once, with individual brakes engaging when each pin is at its desired height. The disadvantage of this approach is that the display is not interactive, but rather of the static refreshable type. That is, for one pin to change its height, the entire display must be reset. A mechanical brake-based display with thousands of pins was previously developed by Xenotran [24]; however, these mechanical clutches require relatively complex manufacturing and assembly making the system expensive. Peters *et al.* [25] also created a brake-based tactile display using a fusible alloy clutch, but the refresh rate of such a device is limited due to the time required to reheat the alloy elements.

In this paper, we present our work on a new static refreshable 2.5D tactile shape display based on electrostatic adhesive brakes. We detail the design, modeling, and fabrication of an individual electrostatic adhesive brake mechanism. We demonstrate two levels of high spatial resolution enabled by this mechanism, fabricating separate rows with 4 mm and 1.7 mm inter-pin spacing, respectively. We further characterize our electrostatic adhesive brake in a series of experiments measuring its maximum sustainable contact force, robustness, refresh rate, and residual force. Based on the individual mechanism, we demonstrate an electrostatic adhesive brake-based tactile shape display prototype with a 4×2 array of pins. We reduce the display's raw material cost to \$0.11 USD per pin by using a transistor-based solid-state brake (0.09 USD for 57.8 mm^2 of PVDF based dielectric film, 0.02 USD for ON MMBTA42LT1G transistor at qt. of 10,000 and 0.004 USD for sputtered metal electrodes). To further increase the maximum contact force sustainable by each pin during haptic exploration, we develop and evaluate a simple, global compliant mechanical clutch to hold the pins in place once initially positioned via electrostatic adhesion. Finally, we present the results of a user study evaluating shape recognition using our tactile shape display prototype compared to static 2.5D tactile graphics as a control.

II. Design of an Individual Electrostatic Adhesive Brake

A. Background

Electrostatic adhesion, first reported by Johnsen and Rahbek in 1923 [26], is a technique commonly used in industry for semiconductor wafer chucking [27] and chemical vapor deposition [28]. More recently, there has been increased interest in electrostatic adhesion for robotics applications such as wall climbing robots [29] and exoskeletal actuation [30]. In general, electrostatic adhesive forces are generated between a substrate under prehension and an electroadhesive pad made by conductive interdigitated electrodes deposited on the surface of a dielectric material. When engaged, the alternating charges on adjacent electrodes create electric fields that induce opposite charges on the substrate material, resulting in coulombic attraction between the pad and the substrate.

Electrostatic adhesion has several advantages over other clutching techniques. Electrostatic adhesive mechanisms can easily be made in small form factors, at low cost, and with very low weight since the patterned electrodes and dielectric material are very thin. Furthermore, they are solid-state and can be made using traditional electronics fabrication methods (e.g., rollable printing) which ensures minimal cost. When the electrodes are active, current flow in the system is very small (e.g., 60 μA) yielding low power consumption. Additionally, a variety of substrate materials can be used with electrostatic adhesion, both conductive and non-conductive; however, conductive materials such as metals generate larger attractive forces.

Specifically, in our design we use electrostatic adhesion to clutch 1.6 mm square brass pins to custom interdigidated electrode pads on a dielectric film fabricated using gold sputtering and laser ablation, as shown in Fig. 1.

B. Modeling

We provide a theoretical model to understand design space of our electroadhesive (EA) brake. The electroadhesive force exerted by the electrodes is modelled using a simplified 2D representation of the Maxwell stress tensor method [31], [32]. Neglecting the effects of magnetism, the electrostatic Maxwell stress tensor T_{ij} is defined in component form as:

$$T_{ij} = \epsilon\left(E_i E_j - \frac{1}{2}\delta_{ij}||\mathbf{E}||^2\right) \quad (1)$$

where ϵ is the dielectric permittivity, δ_{ij} is the Kronecker delta, $\mathbf{E}$ is the electric field in dielectric layer, and E_i and E_j are its ith and jth components, respectively. The electric can be readily calculated from the electric potential Φ as:

$$\mathbf{E} = -\nabla\Phi \tag{2}$$

where Φ must also satisfy the Laplace equation $\nabla^2\Phi = 0$.

We focus our analysis on a single period of the interdigital electrode structure (i.e., *s*+*w* in Fig. 1). The electroadhesive normal force $f_{EA,N}$ per unit width of pin can then be calculated as:

$$\begin{aligned} f_{EA,N} &= \oint_S T_{zz}\, dS \\ &= \frac{1}{2}\epsilon_0 \int_0^{w+s} [E_x^2(x,y,t) - E_y^2(x,y,t)]dx \end{aligned} \tag{3}$$

where ϵ_0 is the permittivity of air, w is the electrode width, s is the gap width between two electrodes, and E_x and E_y are the spatio-temporally varying electric field components.

Note that this model assumes a uniform electric field in the z-direction, and edge effects of the electrode array are neglected. Also note that time-varying characteristics of the electric field are considered here to account for its dynamic response to a step voltage applied to the electrode. When a step voltage is applied, the EA force between the pad and substrate increases over time until saturation (when $F_{EA,N}$ is maximum). This dynamic polarization further creates a time-varying air gap $d_a(t)$ between the EA pad and pin.

The total EA normal force $F_{EA,N}$ across n electrode periods exerted on a pin of width l is subsequently found by:

$$\begin{aligned} F_{EA,N} &= n * l * f_{EA,N} \\ &= \frac{1}{2} n\epsilon_0 l \int_0^{w+s} [E_y^2(x,y,t) - E_x^2(x,y,t)]dx \end{aligned} \tag{4}$$

If the pin is not grounded (as in our case) and dielectric breakdown effects are considered, following [31] we then have:

$$\begin{aligned} F_{EA,N} &= \frac{1}{2} n\epsilon_0 l \left[\left(\frac{\epsilon_r}{\epsilon_0} \right)^2 - 1 \right] \bar{C}(\tilde{w}, \tilde{d}) (E_{BD}^{air})^2 \\ &\text{where} \quad \tilde{w} \equiv \frac{w}{w+s}, \quad \tilde{d} \equiv \frac{2(d+d_a)}{w+s} \end{aligned} \tag{5}$$

where ϵ_r is the relative permittivity of the dielectric film, E_{BD}^{air} is the breakdown electric strength of air, and $\bar{C}(\tilde{w}, \tilde{d})$ is defined as a dimensionless function of geometric parameters comprising the electrode width w, the interelectrode spacing s, the air gap between the dielectric film and the pin d_a, and the thickness of the the dielectric film d. As detailed in [31], the larger the applied voltage and permittivity of the dielectric film, and the smaller the interelectrode spacing, air gap and film thickness, the greater the obtainable EA normal force.

In tactile display applications, the brake is expected to experience non-negligible tangential forces. The maximum contact force supported by an engaged pin is determined by the maximum shear force $F_{EA,S}$ supported by the engaged EA brake, which can be expressed as:

$$\begin{aligned} F_{EA,S} = \mu(F_{EA,N} + F_{Suc} + F_{Van} + F_{Res}\cos\theta) \\ + F_{Res}\sin\theta \end{aligned} \tag{6}$$

where μ is the coefficient of static friction (typically > 1 for most EA surfaces), F_{Suc} is the suction force between the EA pad and pin due to negative pressure, F_{Van} is the Van Der Waals force between the EA pad and pin (F_{Suc} and F_{Van} are typically negligible, however), F_{Res} is the restriction force occurring due to the shear displacement of the EA pad, and θ is the angle between $F_{EA,N}$ and F_{Res}. Since $F_{EA,N}$ is proportional to both pin width and length, increasing these parameters is one way to further increase $F_{EA,S}$.

The theoretical formulation above provides reasonable guidelines for interdigital electrode design in tactile applications. However, there are some trade-offs between these design parameters that prevent us from arbitrarily increasing the maximum allowable contact force ($\approx F_{EA,S}$). Most prominently, although increasing the pin's width or length increases $F_{EA,N}$ (and thus $F_{EA,S}$), it leads to a larger form factor and lower spatial resolution of the tactile display. Furthermore, higher voltages may be at odds with safety considerations as users come into direct contact with the system. Other considerations include the increased cost with higher dielectric constant materials, reduced material strength with reduction in film thickness d, and increased residual force in the disengaged brake with larger friction coefficient μ. In our design evaluation of the electrostatic adhesive brake, we test multiple combinations of these parameters to find a good balance between contact force, cost, spatial resolution, and residual force.

C. Implementation

Fig. 1(a) shows a diagram of an individual electroadhesive brake. In general, an individual brake consists of:

- a 1.6 mm square brass pin (140 mm length)
- a Delrin frame with a 1.90 mm wide by 1.21 mm deep rectangular groove to accept the pin and serve as the primary mechanical structure
- a dielectric film (PolyK Technologies PVDF-TrFE-CFE, $\epsilon_r = 50$) with interdigital electrodes deposited through gold sputtering and laser ablation
- 2 custom side-mounted printed circuit boards (PCBs) that route signals between the interdigital electrodes and a main control board

While not shown in Fig. 1, a linear actuator (Actuonix L12-50-50-6-P) moves a 3D-printed staging platform below the pins to position them prior to engaging the electroadhesive brake. Breakout pads deposited on the dielectric film connect to pads on the PCBs through conductive tape. The trace width of the interdigital electrodes were selected as 500 μm, following results from [34]. The PCBs are 0.5 mm thick to minimize the row-to-row pitch of the tactile display.

To control brake engagement, the circuit shown in Fig. 3 is used. A high voltage transistor (STMicroelectronics STN0214) switches one electrode between a high voltage (engaged) and

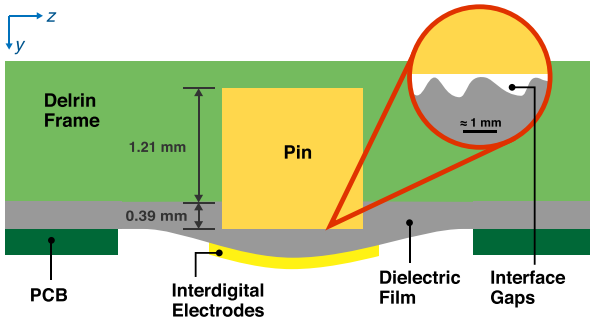

Fig. 2. Top view of an individual electrostatic adhesive brake. The dielectric film is attached to the sides between the frame and two PCBs used to send signals to the electrodes. Overhang of the pin tensions the film and reduces gaps. (Modified from [33], Fig. 4, ©2018 IEEE.)

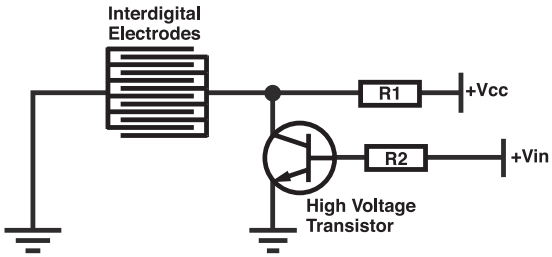

Fig. 3. Circuit schematic of individual electrostatic adhesive brake. A high voltage transistor controls the voltage applied to the electrodes (Vcc), with a series resistor R1 used to limit current. The control signal Vin is sent via microcontroller. (Modified from [33], Fig. 7, ©2018 IEEE.)

ground (disengaged); the complementary electrode is fixed at ground potential. A high voltage DC-DC converter (EMCO AG05p-5) shifts applied voltages from 1.4-2 V to 250-335 V. A resistor (R1 in Fig. 3) is used to limit current in the system. We explore both large (5 $\mathrm{M}\Omega$) and small (i.e., 2.7 $\mathrm{k}\Omega$) values for R1. The larger restricts current below 60 μA when the brake is off, lowering the power consumption (at 300 V) of an individual brake to 1.8 mW and improving safety. The smaller R1 value allows a larger charging current, enabling faster brake engagement as measured in Section II-F. To maximize contact between the pin and dielectric film, the groove in the Delrin frame is made 0.39 mm shallower than the pin. This slight protrusion, as shown in Fig. 2, tensions the film against the pin, minimizing air gaps in the interface and thus increasing the electroadhesive force generated.

To demonstrate the potential for the mechanism's miniaturization, we also fabricate a row of electroadhesive brakes with 0.8 mm brass pins and 1.7 mm pitch, shown in Fig. 4.

In the following sections, we detail a series of experimental evaluations used to characterize the effects of altering design parameters (e.g., voltage, electrode spacing, etc.) on the brake's performance (e.g., electroadhesive force generation, engagement time, etc.). All evaluations were performed using the 1.6 mm pin setup.

D. Evaluation: Quasi-Static Loading

Contact with the user's fingertip is the core element of interaction with any tactile display. Thus, it is important for a

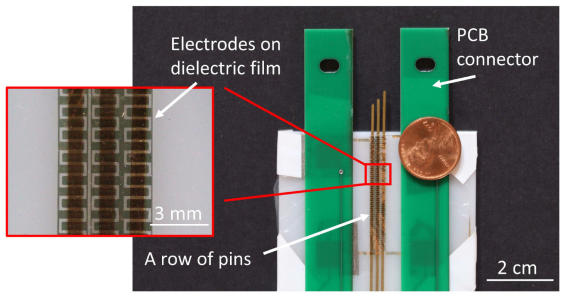

Fig. 4. A high-resolution row of electrostatic adhesive brakes, with a pitch of 1.7 mm and 0.8 mm pins. Inset shows interdigital electrodes fabricated via laser ablation on a 8 μm dielectric film. (From [33], Fig. 1(A), ©2018 IEEE.)

tactile display to support the loads provided by the fingertip as the user explores the display surface. In this section, we ran three experiments to evaluate the effects of interelectrode spacing, dielectric film thickness and electroadhesive brake's resolution on the brake's maximum sustainable contact force before pin slippage. Above parameters are chosen to encompass the most important parameters in our theoretical model (Eq. (5)). These measurements help us better understand ability and design space of our electroadhesive brake to provide large sustainable contact force.

1) Apparatus & Procedure: The setup of this experiment is shown in Fig. 5(a). We simulate the scenario of a fingertip touching the pin using a rate-controlled (2.6 mm/s) linear actuator (Actuonix L12-50-50-6-P) mounted with a force sensor (Honeywell FSG005, 9.8 mN sensitivity). To limit the effects of gravity, the experiment is carried out horizontally, with a single pin laying in a groove of the support frame. As the end-effector of the actuator encounters the pin, the magnitude of the measured contact force increases. As the actuator continues to push on the pin, the measured force increases until the pin begins to slip reletative to the dielectric film and the force drops – we take the maximum force sensor reading prior to slipping as the maximum contact force $F_{C,\max}$ sustainable by the pin.

We ran three experiments: (1) comparing the effect of interelectrode spacing (150 μm, 300 μm, 500 μm) on $F_{C,\max}$, (2) comparing the effect of dielectric film thickness (8 μm, 24 μm) on $F_{C,\max}$, and (3) comparing $F_{C,\max}$ for a high resolution brake (0.8 mm pin width, 1.7 mm pitch) to that of a lower resolution brake (1.6 mm pin width, 4 mm pitch). All experiments were conducted across a range of voltages (50-340 V) with a fixed electrode length of 60.3 mm.

2) Results: The results of these experiments are shown in Fig. 5(b), (c) and (d), respectively. Smaller interelectrode gaps and larger voltages yielded larger $F_{C,\max}$ values. The thinner dielectric film (8 μm) yielded larger $F_{C,\max}$ for voltages below 200 V, while the thicker film (24 μm) yielded larger $F_{C,\max}$ at higher voltages (60% increase at 300 V). The higher resolution brake (0.8 mm pin width, 1.7 mm pitch) supports a decent amount of shear contact force (41 gf at 294 V, 52 gf at 335 V) considering its small form factor. For comparison, the friction force on the pin when the brake was not engaged was measured to be 0.7 gf.

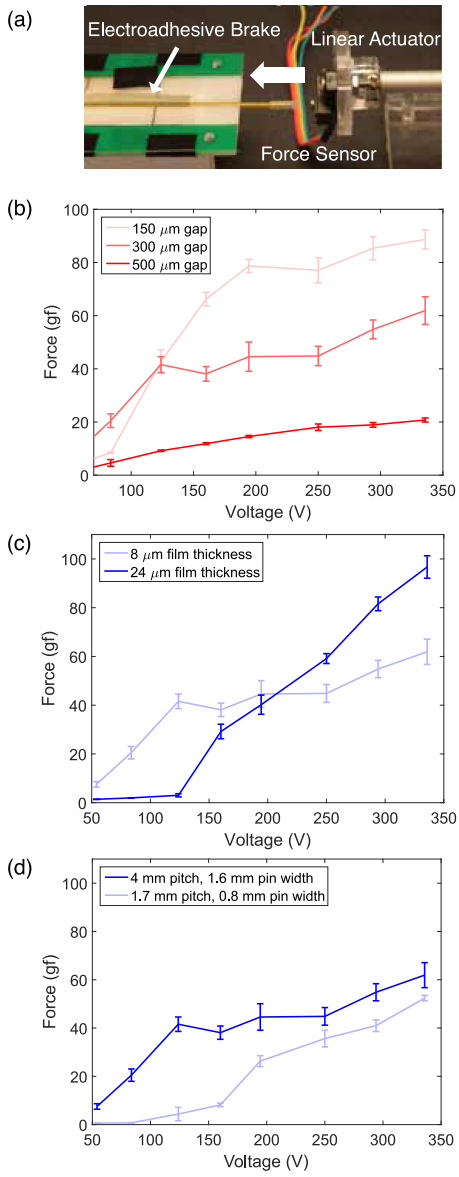

Fig. 5. (a) Experimental setup for contact force measurement. A linear actuator slowly engages the clutched pin and force is measured until brake failure. (b) Maximum contact force of an electroadhesive brake as a function of interdigital electrode spacing. 150 μm, 300 μm and 500 μm gap were investigated. (c) Maximum contact force of an electroadhesive brake as a function of dielectric film thickness. 8 μm and 24 μm thickness were investigated. (d) Maximum contact force of an electroadhesive brake as a function of brake resolution. A higher resolution brake (0.8 mm pin width, 1.7 mm pitch) and a lower resolution brake (1.6 mm pin width, 4 mm pitch) were investigated. Three trials were performed for each condition, with standard deviation shown.

3) Discussion & Parameter Selection: As we can observe from Fig. 5, our measurement results are consistent with our theoretical model's qualitative prediction in Section II-B. The larger the applied voltage, the larger the pin widths, the smaller the interelectrode spacing and the smaller the film thickness (for voltages below 200 V), the larger the sustainable contact force. We will discuss more details of each measurement in following paragraphs.

As shown in Fig. 5(b), higher contact force is observed for smaller interelectrode spacing which is consistent with theoretical analysis results in [31]. However, we cannot further reduce interelectrode spacing to increase contact force because during preliminary testing it was found that spacing smaller than 100 μm produced sparks between the electrodes when 300 V was applied, which can damage the dielectric film and be hazardous to users. Although 150 μm spacing interelectrodes yields largest contact force in our measurement, we selected an interelectrode spacing of 300 μm in our tactile display design to ensure an adequate safety factor,

We also see that rate at which contact force grows with respect to voltage decreases as the applied voltage grows. Given the results of these experiments, we chose to use a voltage of 300 V for our system as it supports sufficiently high contact loads while minimizing the risk of sparking, charge accumulation issues, and higher cost components.

As shown in Fig. 5(c), we also measured the maximum contact force for different dielectric film thicknesses. While a thicker film (24 μm) supported larger contact forces in the 300 V range, for cost and assembly considerations we select a dielectric film thickness of 8 μm.

Although a individual higher resolution brake with 0.8 mm pin width provides a smaller contact force as shown in Fig. 5(d), it has a higher density of pins in a fixed contact area with user's finger, thus being very promising for a high resolution tactile shape display (1.7 mm pitch with 0.8 mm pin width).

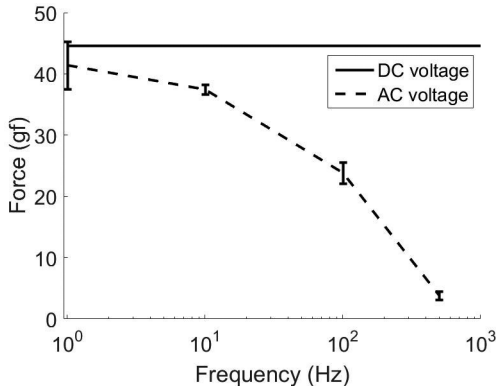

Fig. 6. Comparison of maximum contact force provided DC and AC voltage applied on interdigital electrodes. All measurements are carried out under a voltage of 194.4V, using 60.3 mm length interdigital electrodes, a 1.6 mm width brass pin, and 8 μm thickness dielectric film.

E. Evaluation: AC vs. DC Current

It has been shown that using AC voltage can reduce residual attractive forces in electrostatic adhesion applications by reducing charge accumulation [34]. Here we examine the effect of current type and frequency on the maximum contact force sustained by the brake. Using the same experimental setup as detailed in Section II-D1, we measure the maximum contact force for multiple current frequencies. We use a voltage of 194.4 V, interdigital electrode length of 60.3 mm, and a 1.6 mm width brass pin. Results are shown in Fig. 6, and indicate that contact force decreases with increased AC current frequency. In all cases, DC voltage yielded the largest contact force. For this reason, we select DC current operation for our electrostatic adhesive brake.

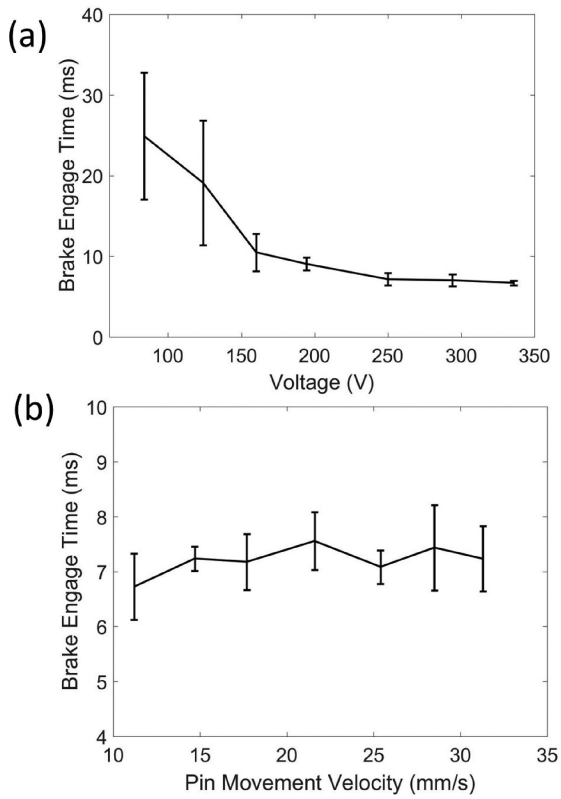

Fig. 7. Brake engage time measurement. All measurements are carried out using 60.3 mm length interdigital electrodes, a 1.6 mm width brass pin, and 8 μm thickness dielectric film. (a) Engagement time as a function of applied voltage. (b) Engagement time as a function of pin velocity. Voltage applied was 294 V.

F. Evaluation: Brake Engagement Time

1) Modeling: The engagement time of our electrostatic adhesive brake is dependent on multiple factors including the electrical aspects as well as mechanical deformation of the film to come in to close contact with the pin. The first we discuss is the charging characteristics of the brake, which we model as a simple capacitor. The schematic in Fig. 13(a) shows that when the brake is engaged, the system can be approximated as a simple RC circuit, with current flowing through a pull-up resistor to charge the interdigital electrodes. Thus, charging time can be approximated given the RC time constant of the circuit. We estimate the capacitance of the brake using the following equation:

$$C = \epsilon_r \epsilon_0 \frac{A\eta}{d} = \epsilon_r \epsilon_0 \frac{w h_{contact} \eta}{4d} \tag{7}$$

where η is the percentage of non-conductive area on the electrode pad, w is the pin width, and $h_{contact}$ is the length of pin in contact with electrodes. In our system, we have η = 62.5%, w = 1.6 mm and $h_{contact}$ = 60.3 mm. This corresponds to a capacitance of 0.82 nF. We use a 2.7 $k\Omega$ resistor in series to charge the electrodes; thus, the RC time constant is 2.2 μs.

While this value estimates the time to electrically charge the brake, mechanical properties such as air gap in the pin-film interface and wrinkles of film also play an very important role. Since these properties can vary with time thus difficult to model, we perform an experimental investigation to quantify the total brake engagement time for our mechanism.

2) Apparatus & Procedure: The experiment was conducted using a single pin electroadhesive brake vertically mounted. The pin was modified with a light conductive element mounted to the bottom, which bridged two small conductive plates on the actuator platform when the pin was resting on it. With the brake disengaged, the pin was driven down by the actuated platform at a constant speed. The brake was then engaged, and the time difference between switching the voltage on (t_1) and the pin separating from the downward-traveling platform (t_2) was measured to be the brake engagement time. t_1 was captured in software after sending the brake command and t_2 was found by measuring the electrical connectivity between the actuator plates.

Since the actuator speed used to raise and lower the pins is potentially a large factor in determining the refresh rate of a brake-based tactile display, we also characterize brake engagement time for various actuator speeds as well as voltages.

3) Results & Discussion: Fig. 7(a) shows the results of varying applied voltage on engagement time of the electrostatic adhesive brake. The pin was lowered at 12.1 mm/s in this experiment. Intuitively, larger voltage leads to larger attractive forces, which leads to faster brake engagement. For 335 V, the largest voltage tested, we observed an engagement time of 6.7 ms. We also note that for smaller voltages (below 200 V) measured engagement time was much less consistent, indicated by the large standard deviation bars. Moreover, the experimentally determined engagement time (6.7 ms @ 335 V) is significantly larger than the calculated electrical time constant (2.2 μs), indicating that unmodeled mechanical factors play a dominant role in dictating engagement time for the brake.

Fig. 7(b) shows brake engagement time measured as a function of actuation velocity. As the results show, brake engagement did not show significant variation across a velocity range of 11 to 31 mm/s when measured for a voltage of 294 V (all roughly 7 ms). By using higher actuation speeds, the refresh rate of an overall display can be increased.

G. Evaluation: Residual Force

When refreshing the tactile shape display, voltage to the electrodes is switched off and the electrostatic attraction force between the pin and film dissipates, allowing the pins to detach. Ideally, this process is instantaneous and no force is acting on the pin once the brake is off. In practice, however, some residual electrostatic force remains even after the electrodes are off. Since each pin is very light (1 gf), these residual forces may have a significant effect on system performance (e.g., creating unwanted impedance when resetting the display). Thus, we characterized the residual force in an individual brake for a range of applied voltages, as shown by Fig. 8.

The experimental setup was identical to that in Section II-D. Residual force was measured as the average resistance experienced by the actuator driving the pin at 2.6 mm/s after the

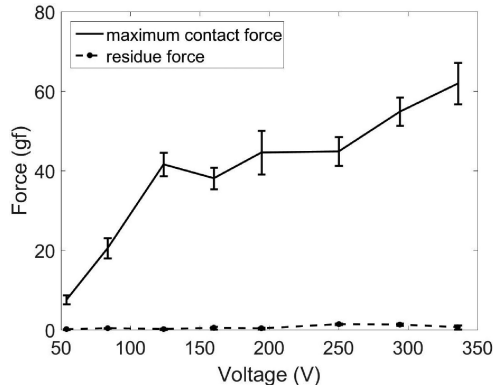

Fig. 8. Maximum contact force and residue force observed for different applied voltages. Maximum contact force is measured with the electrodes turned on, while residual force is measured with the electrodes just switched off. All measurements are carried out using 60.3 mm length interdigital electrodes, a 1.6 mm width brass pin, and 8 μm thickness dielectric film.

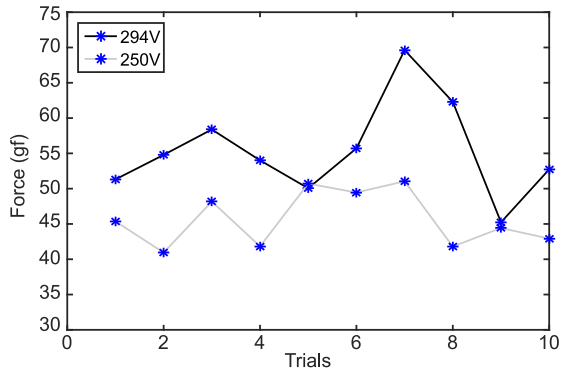

Fig. 9. Repeatability of maximum contact force sustainable by an electroadhesive brakes is evaluated over ten trials, with electrostatic discharging of the pin after each trial. All measurements are carried out using 60.3 mm length interdigital electrodes, a 1.6 mm width brass pin, and 8 μm thickness dielectric film.

TABLE I
STATIC LOADING ROBUSTNESS TEST

Experiment	Load	Cycles Until Failure
1*	1 gf	4740
2**	13 gf	over 1021
	18 gf	over 1021
	23 gf	80

*Failure considered unsuccessful attachment of pin to film, or failure to detach from film when brake disengaged. Carried out with a voltage of 294 V. Weight of pin alone is 1 gf. **Failure considered pin detachment from film and/or significant slippage. Carried out with a voltage of 318 V.

electrodes were turned off. Interdigital electrodes with a total length of 60.3 mm and a 1.6 mm square pin were used in this experiment.

The friction force between the pin and Delrin frame alone was previously measured to be 0.7 gf; this is subtracted from all measurements to obtain the contribution from residual force alone. The average electrostatic residual force measured across all tested voltages is 0.6 gf. Thus, total resistive force in the brake after switching off the voltage is 1.3 gf. Furthermore, higher residual force is observed for higher applied voltages.

H. Evaluation: Robustness

1) Static Loading Robustness: In the context of a tactile shape display, it is important that our electrostatic adhesive brake mechanism to repeatedly and reliably (1) attach and support the pins (1 gf) when engaged and (2) handle the loads imparted by fingers repeatedly making contact. We conduct two experiments to evaluate these conditions. In both experiments, the brake setup was mounted vertically. In the first experiment, a pin is repeatedly attached to the film via engagement of the brake and reset using the global actuation platform. An electrically grounded pad on the actuation platform is used to reduce charge accumulation. The goal of this experiment is to observe the number of cycles achieved before failure (i.e., unsuccessful pin attachment or failure to detach due to residual adhesion build up). We observed failures of pin detachment after 4740 cycles of successful loading and unloading of the pin (see Table I, Experiment 1). This is due to increasing residual adhesion during the course of the test which can be mitigated after resting the device [35]. No failure of pin attachment is observed during the test. The experiment was carried out with a voltage of 294 V.

The second experiment evaluated the repeated loading/unloading of an attached pin. Three calibration weights were tested: 13 gf, 18 gf, and 23 gf. In this experiment, a calibration weight was hung on the bottom of the pin with fishing line and the brake was engaged. The actuation platform was raised and lowered cyclically to repeatedly load and unload the hanging weight from the pin. In the unloaded state, the weight was supported by the platform; in the loaded state, the weight hung freely from the pin. We report the number of cycles observed before failure (i.e., pin detachment). The experiment was carried out with a voltage of 318 V. The results of the two experiments are compiled in Table I. We observed no failure in the repeated loading of 13 gf and 18 gf calibration weights after 1021 cycles. In the 23 gf case, we observed failure after 80 cycles. These results indicate the electroadhesive brake can reliably function and sustain expected contact loads over time.

2) Maximum Contact Force Repeatability: To further characterize the robustness of our electrostatic adhesive brake, we also measure the consistency of the maximum contact force observed over multiple trials. The experimental setup is identical to that in Section II-D; here the procedure is repeated for a fixed voltage and changes in the maximum contact force are observed over 10 trials. The brass pin is discharged using conductive fabric after each trial to prevent charge accumulation. Interdigital electrodes with a total length of 60.3 mm and a 1.6 mm square pin were used in this experiment.

The results of this experiment are shown in Fig. 9. Although the maximum contact force shows some variation over 10 trials (STD 3.89 gf for 250 V, STD 6.81 gf for 294 V), the observed minimums of 40.9 gf (250 V) and 45.2 gf (294 V) indicate the brake would still support contact forces expected during haptic exploration.

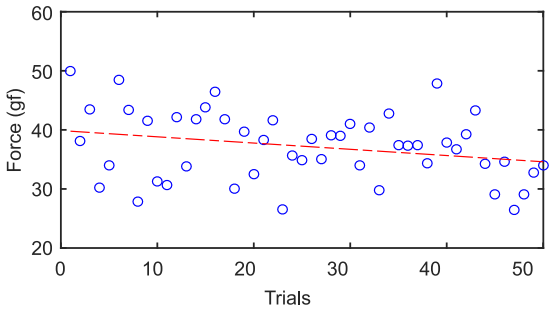

Fig. 10. Repeatability of maximum contact force sustainable by an electroadhesive brakes is evaluated over 50 trials, without discharging the pin after each trial. We observe a slight decreasing trend in magnitude (red) due to charge accumulation in the brake. All measurements are carried out using 60.3 mm length interdigital electrodes, a voltage of 294 V, a 1.6 mm width brass pin, and 8 μm thickness dielectric film.

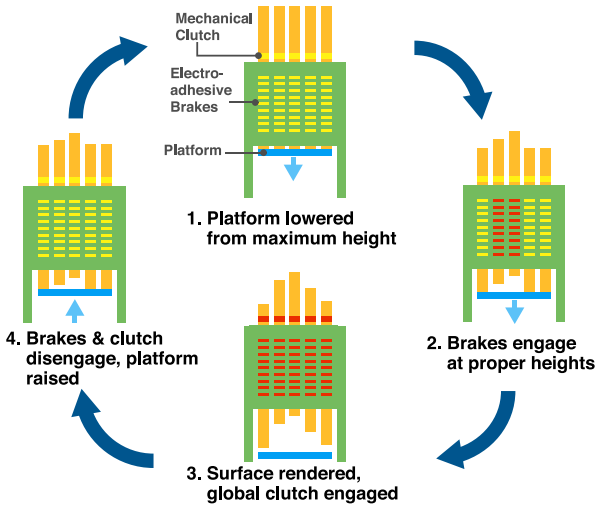

Fig. 11. Rendering workflow of an electroadhesive brake-based refreshable tactile display. An actuated platform positions the pins which are then clutched via electroadhesive braking. When the surface is complete, a global mechanical clutch can be engaged to further increased the holding force on the pins. Red indicates brake/clutch engagement.

3) Charge Accumulation & Contact Force Degradation: Charge accumulation is a known challenge in electroadhesive force applications that can cause performance issues. When a user's fingertip contacts the tactile display with significant force, relative movement between the pin and electrodes will induce a charge buildup in the brass pin. To asses the effect of this charge accumulation on the maximum contact force sustainable by our electroadhesive brake, we perform an experiment identical to that in the preceding section except we did not discharge the pin between trials to remove accumulated charge.

The results of this experiment are shown in Fig. 10. We see that contact force tends to degrade with repeated trials, decreasing by approximately 10% after 50 trials of loading until failure. As will be discussed in Section III-B, a mechanical clutch is developed to increase the contact force sustainable by each pin after initially attached using electrostatic attraction. Thus, relative motion between pin and film is further minimized, and the effect of charge accumulation is less severe.

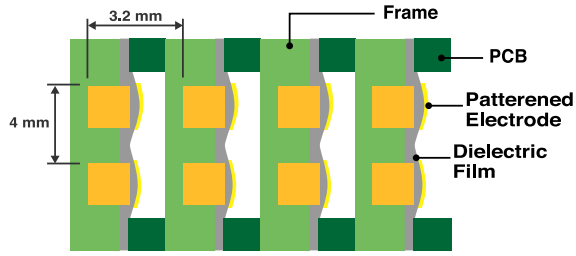

Fig. 12. Top view of the tactile display prototype. Pitch size is 4 mm within-row and 3.2 mm between-row. Milled Delrin sheets are used to constrain the pins, and side-mounted PCBs connect the interdigital electrodes to a main control board.

III. Design of a 2.5D Tactile Display Using Electrostatic Adhesive Brakes

A. System Workflow

In this section, we introduce the basic operating process of an electroadhesive brake-based refreshable tactile shape display. This workflow is illustrated by Fig. 11. Initially, all brakes are disengaged and all pins are resting on the global actuation platform. The platform is first raised to its maximum height, and then lowered (Fig. 11.1). Driven by gravity, the pins follow the platform's movement downward. During this process, individual electroadhesive brakes engage to clutch each pin at their desired heights (Fig. 11.2), leaving the desired 2.5D surface rendered (Fig. 11.3). To further increase the maximum contact loads supported by the rendered surface, a global mechanical clutch (described in Section III-B) can engage all pins once the surface is rendered. To refresh the display, the mechanical clutch is disengaged, followed by all electroadhesive brakes. The platform is then raised to its highest position, physically disengaging any pins that may remain clutched due to residual electrostatic adhesion (Fig. 11.4). If rendering another surface, the process then begins again with a different set of desired pin positions.

B. System Design and Implementation

To demonstrate the the potential for electroadhesive braking in high resolution shape rendering applications, we designed a 4×2 tactile shape display prototype shown in Fig. 14.

1) Mechanical Assembly: A top view schematic of the display is illustrated in Fig. 12. The main structure is composed of four layered Delrin sheets (1.98 mm thick), each with two pin grooves (1.90 mm wide, 1.21 mm deep, 4 mm spacing) milled using a desktop CNC (Bantam Tools Desktop PCB Milling Machine). Square brass pins (1.6 mm) in each row are constrained between the grooves and a dielectric film (8 μm, PolyK Technologies PVDF-TrFE-CFE). Two pairs of interdigital electrodes deposited on each dielectric film through gold sputtering and laser ablation enable individual braking of each pin. The dielectric film is tensioned and fixed to the sides of the Delrin layer via adhesive. A custom PCB lines each side of the layer, routing signals from a master control board to breakout pads on the dielectric film via a thin layer of conductive tape. The two PCBs, dielectric film, milled Derin sheet, and two pins

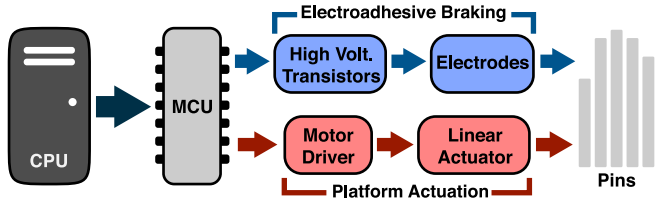

Fig. 13. System diagram of our tactile shape display. The CPU forwards desired pin positions to a microcontroller over USB Serial, which then sets the display accordingly by driving an actuated platform and applying the electroadhesive brakes at the proper heights.

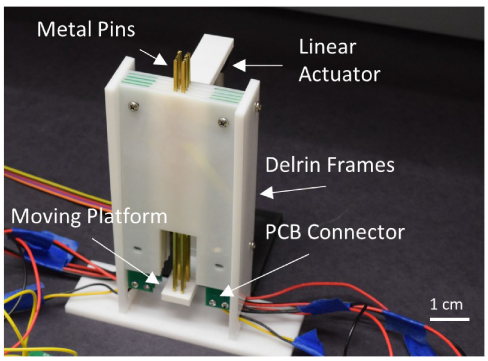

Fig. 14. Prototype tactile shape display. A single actuated platform moves pins into position for braking. PCBs in each row route signals between the electrodes and transistors on a separate board. (From [33], Fig. 8, ©2018 IEEE.)

make up a single row of the display. Rows are then stacked with 3.2 mm spacing to create a 4×2 pin array.

2) Electronics & Control: Signals to the interdigital electrodes are governed by a control board consisting of a microcontroller (PJRC Teensy 3.6), 9 high voltage transistors (STMicroelectronics STN0214), a high voltage DC-DC converter to shift voltages from 1.4-2 V to 250-335 V, and a motor driver (TI DRV8833) for controlling a global actuation platform. An individual control circuit diagram for a single electrostatic adhesive brake is shown in Fig. 3. A 5 MΩ current-limiting resistor is used in each brake to keep current below 60 μA for safety considerations. An overall system diagram is shown in Fig. 13.

3) Actuation: To actively raise and lower pins within the display, a global actuation platform is used. A linear actuator (Actuonix L12-50-50-6-P) is fit with a 3D printed platform beneath the pins and drives them to their desired heights prior the brakes engaging.

C. Mechanical Clutch

With the setup as-described, the entire 4×2 tactile array can support approximately 300-400 gf of contact force when operating at 300 V, assuming all pins are contacted equally. The main limiting factor for this contact force stems from the small form factor of the pins, which is necessary for high spatial resolution. To address this trade-off and enable our display to support larger forces, we developed a global mechanical

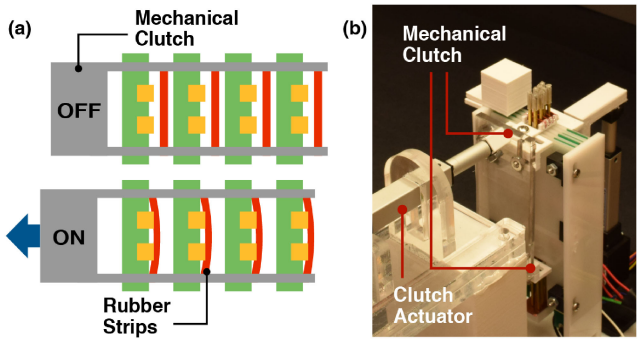

Fig. 15. (a) Diagram of mechanical clutch design. When engaged, rubber strips clutch all pins in place and allow the surface to sustain higher contact forces. (b) Assembled mechanical clutch and tactile display. Two linked clutches are used (top and bottom) to avoid asymmetric loading.

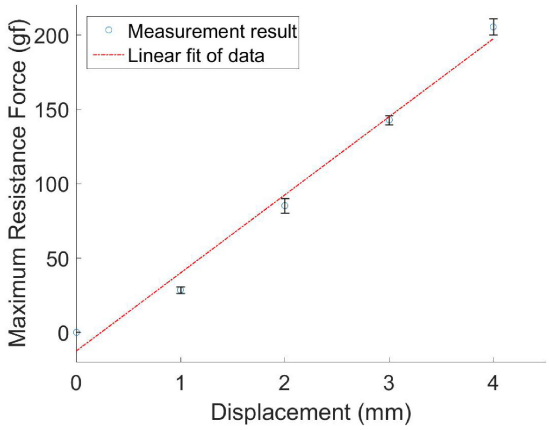

Fig. 16. Measured maximum contact force sustained by mechanically-clutched pin and corresponding linear fitting of the measured data.

clutch to clutch all pins in place after positioning via actuation platform/electroadhesive braking. Shown in 15(a), the clutch is designed with two main elements: a 3D printed structural frame, and a series of compliant silicone rubber strips (McMaster-Carr 3788T21) which engage the pins. A second linear actuator (Actuonix L12-50-50-6-P) is used to retract the mechanical clutch such that the rubber strips engage the pins and provide significant additional friction and holding force. To prevent asymmetric loading on the pins, two identical mechanically coupled clutches are used on the top and bottom of the pin array.

1) Evaluation of Mechanical Clutch: We experimentally evaluate the additional contact force sustained by our mechanical clutch. We measured the maximum contact force supported by all 8 pins engaged at once for different mechanical clutch displacements. In this evaluation, only the mechanical clutch was engaged; no electrostatic adhesion was used. The results of this experiment are shown in Fig. 16. A linear fit of the measured data yields a slope of 52.5 gf/mm, an intercept of -12.7 gf, and an R^2 value of 0.9852 indicating that our clutch can be modeled reasonably well as a simple spring. That is, the maximum contact force sustained by the clutch can be estimated as linearly proportional to its displacement.

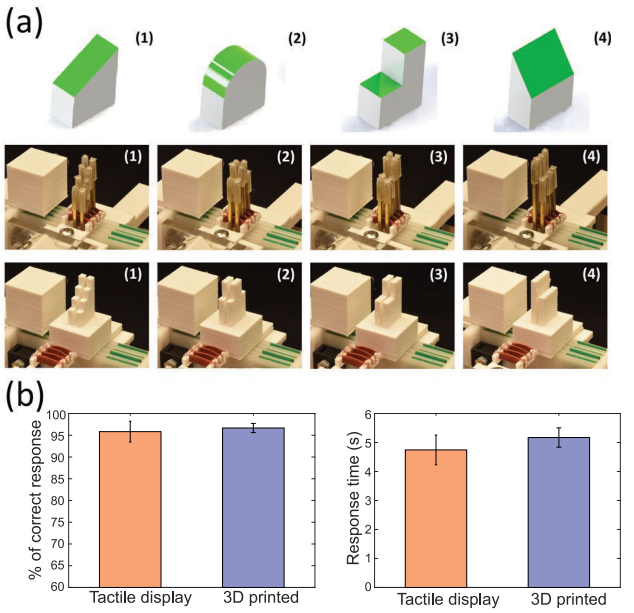

Fig. 17. (a) Shapes rendered in the user study. Top: images shown to user during the study. Middle: corresponding 2.5D shapes rendered by our tactile display. Bottom: 3D printed shapes used as a control. (b) Results of the study comparing shape recognition rates and response times between the tactile display and 3D printed conditions. Error bar depicts standard error in results.

From these results, we observe that the mechanical clutch yields a maximum contact force of 211 gf when engaged with 4 mm displacement. The addition of this force on top of that supplied by the electrostatic adhesive brakes helps ensure the tactile display can support contact loads from the fingertip during haptic exploration (51 gf of contact force is sufficient for small feature exploration according to [13]), and can especially help combat issues with electroadhesive force degradation due to charge accumulation that are present with the electrostatic adhesive brakes alone.

D. System Refresh Rate Analysis

Considering the rendering workflow detailed in Section III-A, if a refreshable tactile display has n pins, then there at most n different pin heights in a given rendering. As experimentally characterized in Section II-F, the engagement time of a single electrostatic adhesive brake is approximately 6.7 ms when using 335 V. Thus, the display would require at least $6.7 \times n$ ms to engage all pins, not considering travel time between pin heights. In the case of our prototype display, this value is $6.7 \text{ ms} \times 8 \text{ pins} = 54.6 \text{ ms}$.

As experimental results showed in Section II-F, the electrostatic adhesive brakes can be engaged without the actuation platform coming to a stop (11-31 mm/s tested). Meaning, to render any surface the actuation platform would simply need to travel from its uppermost to its lowest position, with the pins being electrostatically clutched individually at their appropriate heights (see Fig. 11.2); hence, the speed of the actuation platform is the dominant factor determining the overall refresh rate of the display. Considering a dynamic height range of 50 mm for a given display, a platform linearly actuated at 30 mm/s could render a surface in 1.67 s. To refresh the display, the platform must move up another 50 mm, corresponding to another 1.67 s. Thus, the total rendering time for any arbitrary surface is considered to be 3.33 s, yielding a refresh rate of 0.3 Hz. A faster linear actuator and reduced dynamic range would further increase the refresh rate of the display at the cost of rendering accuracy and fidelity (e.g., 2 mm dynamic height with 50 mm/s actuator speed will increase refresh rate to 12.5 Hz). According to [3], for applications involving static refreshable tactile displays users typically take a few minutes to explore the entire display, thus around 10 s [3] refresh rate is sufficient (note that our refresh rate does not scale with number of pins). From our refresh rate analysis, our system can readily satisfy the requirements of a static refreshable display.

IV. User Study

We carried out a user study to evaluate our prototype display's effectiveness in representing high resolution 2.5D shapes. As described in [3], static refreshable tactile displays can substitute for nonrefreshable haptic graphics in education, various professional activities, and entertainment applications. Our goal was to determine whether users using our static refreshable tactile display can achieve similar shape recognition performance as with nonrefreshable haptic graphics (i.e., 3D printed patterns). We also aimed to verify that the display is capable of handling the contact forces imparted during haptic exploration. Rather than exploring new areas of haptic perception, our study is mainly carried out to validate the robustness and performance our EA brake-based tactile display. A total of four shape patterns were tested. A set of static 3D printed shapes with identical spatial resolution as our display was used as a control for comparison. The shape patterns, display renderings, and 3D printed models used are shown in Fig. 17(a).

A. Participants

We recruited 6 participants age 20-26 (M = 23, 1 female), five right-handed and one left-handed for this experiment. Participants were compensated at a rate of 15 USD an hour, and with the experiment generally lasting less than an hour.

B. Materials

Our 4×2 prototype shape display was used in this experiment, mounted on a desktop. 3D printed proxy shapes were mounted onto the display during the appropriate conditions. A visual barrier prevented users from seeing the display or their hand during interaction. Images of the four shape patterns (Fig. 17(a), first row) were displayed on a board visible to the user at all times.

C. Procedure

At the start of each study, a short training session was carried out familiarize users with the sensation of tactile shape exploration using the device and 3D printed shapes. During each condition, four shapes were presented to the participant a total of 20 times in a randomized order. Thus each participant

experienced 20 repetitions $\times$ 2 conditions = 40 trials. In each trial, the designated shape was either rendered using the display or the experimenter physically mounted the corresponding 3D printed shape to the display, depending on the condition. When rendered, the participant was instructed to feel the shape and give their best guess as to which of the visible shapes they were touching. Participants were given a short break in between the two conditions. To counteract any learning effects, half of the studies were performed with the tactile display condition first and the other half with the 3D printed proxies condition first, with all participants performing both conditions.

D. Results & Discussion

The results of the study are shown in Fig. 17(b). We observe 95.83% shape recognition accuracy (SE 2.39%) for the tactile display condition, and 96.67% shape recognition accuracy (SE 1.05%) for the 3D printed shape condition. No significant difference between shape recognition in the tactile display and 3D printed cases ($p = 0.7412$); this is intuitive as both the display and the 3D printed shapes have identical spatial resolution.

The primary difference between the two cases is in the amount of contact force they can sustain without deformation. The 3D printed shapes are made of PLA, which is a generally durable and hard material – thus, they can sustain considerable loading and did not deform at all during the study. Conversely, our tactile display can support roughly 75 gf per pin considering clutching force from both the electroadhesive brake (50 gf at 294 V) and mechanical clutch (25 gf with 4 mm displacement). However, the comparable shape recognition accuracy between the two suggests that the tactile display was able to retain its rendered shape without significant deformation during haptic exploration. The larger standard deviation for shape recognition in the tactile display case highlights the impact of individual differences in haptic exploration practices (e.g., how much contact force is applied) and how they may be relevant when designing tactile displays. In both conditions, participants did not achieve 100% accuracy likely due to the fact that they were feeling physically rasterized versions of the shapes they saw (as illustrated by Fig. 17(a)), which are likely easier to confuse. Although temporary brake failure due to overloaded user contact force may jeopardize tactile display performance, we only observed a small (0.8%) accuracy difference between rendered shape and 3D printed shape. No other obvious pin displacements were found. The participants' response times were also comparable in both conditions ($p = 0.4891$), as shown in Fig. 17(b).

As mentioned in Section IV, the purpose of this study is to verify robustness and performance of our EA brake-based device as a functional tactile display. Correctness rate and response time comparable to 3D printed shapes, as shown in Fig. 17, demonstrate our device's ability to repeatably render patterns correctly.

V. Limitations & Future Work

The most salient limitation of the proposed electroadhesive brake is the magnitude of contact force it can support. As shown by Fig. 5, an individual brake can support $\approx$50 gf at 300 V. As our prototype tactile shape display has 8 pins, it can ideally support $\approx$400 gf if the load is equally distributed between pins. We demonstrated a moderate improvement to this load capacity with the addition of a global mechanical clutch, which provides another 200 gf of contact load support; thus, if contact is equally distributed, the prototype display can support $\approx$600 gf, which is more than sufficient for small feature exploration according to [13]. In practice, any occasional pin slippage can also be corrected by refreshing the display. Future work should investigate pin displacement during haptic exploration to confirm the usable resolution in the x-axis of the pin display.

Our proposed brake mechanism also has significant voltage requirements ($\approx$300 V). However, since current requirements are very low (less than 60 $\mu\mathrm{A/pin}$), power consumption by the system is considerably small($\approx$ 18 $\mathrm{mW/pin}$). Furthermore, insulating caps are placed on each pin to ensure user safety when interacting with the system.

The primary limitation of any brake-based tactile display is that shape rendering can not be dynamic; to change the height of a single pin, the entire display must be refreshed. While there are many applications in which a refreshable display is sufficient, such as tactile information displays for the visually-impaired and passive haptic feedback in virtual reality, the ideal tactile shape display would support dynamic rendering, allowing rendered contact to react to user interaction (e.g., pressing a rendered button) and further decreasing rendering time.

Our current design relies on gravity to set and reset pins. This design reduces the structural complexity of our system but also limits the system refresh rate since a pin's acceleration during the refreshing process is bounded by gravitational acceleration. The other limitation is that the device must be oriented such that gravity is aligned with the travel of the pins. However, these limitations may be overcome in future work by developing dynamic control for individual pins in an electroadhesive brake-based display, potentially through the use of multiple sets of interdigital electrodes per pin. Another potential solution is the development of electrostatic linear motors for individual pin control, such as inchworm motors [36]. However, the low output force of these actuators may limit the system's capabilities as a tactile display.

To meet the practical requirements of most real-life tactile applications, scaling the display up from the current 4×2 array (to, say, 100×100) is essential. Replacing manual assembly with a repeatable automated process would largely solve misalignment issues and improve functional consistency. With a larger display, however, the global mechanical clutch design may also need revision to prevent uneven distribution of clutch force. One potential solution is to move from parallel rubber strips to a grid, providing interstitial anchor points between groups of pins. Implementation of both an automated assembly process and a grid-like global clutch design should be experimentally explored in future work.

Although we characterized the maximum contact force supported by a high resolution version of our EA brake-based display in this paper, we have not yet built a larger scale high-

resolution tactile shape display. Since everything will be further miniaturized in this design, our future work will investigate how to fabricate an EA brake structure with 100 μm accuracy. Nanofabrication methods (i.e., lithography) used in Micro-Electro-Mechanical Systems (MEMS) research will be introduced to replace our current fabrication methods (i.e., laser cutting, milling)

Another possible direction is integrating direct sensing of pin heights which can be used to determine if a pin has slipped or was misattached. One approach could be to engineer the system such that the contact area between the pin and electrodes is proportional to its height; pin height could then be sensed directly by measuring the capacitance of the electroadhesive brake.

VI. Conclusion

We presented the modeling, design, and characterization of a low cost, small form-factor, lightweight, low power electroadhesive brake in this work. We evaluated the proposed brake's load capacity, engagement time, robustness, and residual force characteristics. To demonstrate the use of our electroadhesive brake in high resolution tactile shape display applications, we developed a 4×2 electroadhesive brake-based prototype display with 4 mm interpin spacing and 3.2 mm interrow spacing. We detailed the system workflow of our electroadhesive brake-based display, and analyzed the overall refresh rate of the device. We also detailed the addition of a global mechanical clutch to further increase the display's contact load capacity. Lastly, we presented the results of a user study evaluating users' shape recognition accuracy when interacting with our tactile shape display.

Through our investigations, we believe that electrostatic adhesive brakes have demonstrated significant potential for improving the spatial resolution and lowering the cost of static refreshable 2.5D tactile shape displays.

Acknowledgement

Portions of this paper reprinted with permission from [33], ©2018 IEEE.

References

[1] H. R. Choi *et al.*, "Tactile display as a Braille display for the visually disabled," in *Proc. IEEE/RSJ Int. Conf. Intell. Robots Syst.*, 2004, vol. 2, pp. 1985–1990.

[2] G. Petit, A. Dufresne, V. Levesque, V. Hayward, and N. Trudeau, "Refreshable tactile graphics applied to schoolbook illustrations for students with visual impairment," in *Proc. 10th Int. ACM SIGACCESS Conf. Comput. Accessibility*, 2008, pp. 89–96.

[3] F. Vidal-Verdú and M. Hafez, "Graphical tactile displays for visually-impaired people," *IEEE Trans. Neural Syst. Rehabil. Eng.*, vol. 15, no. 1, pp. 119–130, Mar. 2007.

[4] E. Y. Chen and B. A. Marcus, "Exos slip display research and development," in *Proc. Int. Mech. Eng. Congr. Expo.*, 1994, pp. 55–1.

[5] E. Petriu and W. McMath, "Tactile operator interface for semi-autonomous robotic applications," *Proc. Artif. Intell., Robot. Autom., Space*, pp. 77–82, 1992.

[6] C. R. Wagner, S. J. Lederman, and R. D. Howe, "A tactile shape display using RC servomotors," in *Proc. 10th Symp. Haptic Interfaces for Virtual Environ. Teleoperator Syst.*, 2002, pp. 354–355.

[7] M. Benali-Khoudja, M. Hafez, J.-M. Alexandre, and A. Kheddar, "Tactile interfaces: A state-of-the-art survey," in *Proc. Int. Symp. Robot.*, 2004, vol. 31, pp. 23–26.

[8] H. Iwata, H. Yano, F. Nakaizumi, and R. Kawamura, "Project FEELEX: Adding haptic surface to graphics," in *Proc. 28th Annu. Conf. Comput. Graph. Interactive Techn.*, 2001, pp. 469–476.

[9] D. Overholt, "The MATRIX: A novel controller for musical expression," in *Proc. Conf. New Interfaces Musical Expression*, 2001, pp. 1–4.

[10] M. W. Wijntjes, A. Sato, A. M. Kappers, and V. Hayward, "Haptic perception of real and virtual curvature," in *Proc. Int. Conf. Human Haptic Sens. Touch Enabled Comput. Appl.*, 2008, pp. 361–366.

[11] H. Dostmohamed and V. Hayward, "Trajectory of contact region on the fingerpad gives the illusion of haptic shape," *Exp. Brain Res.*, vol. 164, no. 3, pp. 387–394, 2005.

[12] M. Shimojo, M. Shinohara, and Y. Fukui, "Human shape recognition performance for 3D tactile display," *IEEE Trans. Syst., Man, Cybern. A, Syst. Humans*, vol. 29, no. 6, pp. 637–644, Nov. 1999.

[13] A. M. Smith, G. Gosselin, and B. Houde, "Deployment of fingertip forces in tactile exploration," *Exp. Brain Res.*, vol. 147, no. 2, pp. 209–218, 2002.

[14] M. Shinohara, Y. Shimizu, and A. Mochizuki, "Three-dimensional tactile display for the blind," *IEEE Trans. Rehabil. Eng.*, vol. 6, no. 3, pp. 249–256, Sep. 1998.

[15] S. Follmer, D. Leithinger, A. Olwal, A. Hogge, and H. Ishii, "inFORM: Dynamic physical affordances and constraints through shape and object actuation." in *Proc. ACM Symp. User Interface Softw. Technol.*, 2013, vol. 13, pp. 417–426.

[16] J. J. Zárate and H. Shea, "Using pot-magnets to enable stable and scalable electromagnetic tactile displays," *IEEE Trans. Haptics*, vol. 10, no. 1, pp. 106–112, Jan. –Mar. 2017.

[17] I. Poupyrev, T. Nashida, S. Maruyama, J. Rekimoto, and Y. Yamaji, "Lumen: Interactive visual and shape display for calm computing," in *Proc. ACM SIGGRAPH Emer. Technol.*, 2004, Art. no. 17.

[18] M. Nakatani, H. Kajimoto, D. Sekiguchi, N. Kawakami, and S. Tachi, "3D form display with shape memory alloy." in *Proc. 13th Int. Conf. Artif. Reality Telexistence*, 2003, vol. 8, pp. 179–184.

[19] H. Zhu and W. J. Book, "Practical structure design and control for digital clay," in *Proc. ASME Int. Mech. Eng. Congr. Expo.*, 2004, pp. 1051–1058.

[20] T. Ninomiya, K. Osawa, Y. Okayama, Y. Matsumoto, and N. Miki, "MEMS tactile display with hydraulic displacement amplification mechanism," in *Proc. IEEE Conf. Micro Electro Mech. Syst.*, 2009, pp. 467–470.

[21] K.-U. Kyung, M. Ahn, D.-S. Kwon, and M. A. Srinivasan, "A compact broadband tactile display and its effectiveness in the display of tactile form," in *Proc. First Joint Eurohaptics Conf. Symp. Haptic Interfaces Virtual Environ. Teleoperator Syst. World Haptics Conf.*, 2005, pp. 600–601.

[22] S. Jang, L. H. Kim, K. Tanner, H. Ishii, and S. Follmer, "Haptic edge display for mobile tactile interaction," in *Proc. CHI Conf. Human Factors Comput. Syst.*, 2016, pp. 3706–3716.

[23] M. Jungmann and H. F. Schlaak, "Miniaturised electrostatic tactile display with high structural compliance," in *Proc. Conf. Eurohaptics*, 2002, pp. 12–17.

[24] C. Carlberg, "Clutch mechanism for a raised display apparatus," U.S. Patent 7 439 950, Oct. 21, 2008.

[25] B. J. Peters, "Design and fabrication of a digitally reconfigurable surface," Ph.D. dissertation, Department of Mechanical Engineering at the Massachusetts Institute of Technology, Cambridge, MA, USA, 2011.

[26] A. Johnsen and K. Rahbek, "A physical phenomenon and its applications to telegraphy, telephony, etc." *J. Inst. Elect. Eng.*, vol. 61, no. 320, pp. 713–725, 1923.

[27] K. Asano, F. Hatakeyama, and K. Yatsuzuka, "Fundamental study of an electrostatic chuck for silicon wafer handling," *IEEE Trans. Industry Appl.*, vol. 38, no. 3, pp. 840–845, May/Jun. 2002.

[28] R. Chandrasekhar and K. Choy, "Electrostatic spray assisted vapour deposition of fluorine doped tin oxide," *J. Crystal Growth*, vol. 231, no. 1/2, pp. 215–221, 2001.

[29] K. H. Koh, M. Sreekumar, and S. Ponnambalam, "Hybrid electrostatic and elastomer adhesion mechanism for wall climbing robot," *Mechatronics*, vol. 35, pp. 122–135, 2016.

[30] S. Diller, C. Majidi, and S. H. Collins, "A lightweight, low-power electroadhesive clutch and spring for exoskeleton actuation," in *Proc. IEEE Int. Conf. Robot. Autom.*, 2016, pp. 682–689.

[31] C. Cao, X. Sun, Y. Fang, Q.-H. Qin, A. Yu, and X.-Q. Feng, "Theoretical model and design of electroadhesive pad with interdigitated electrodes," *Mater. Des.*, vol. 89, pp. 485–491, 2016.
[32] R. Chen, Y. Huang, and Q. Tang, "An analytical model for electrostatic adhesive dynamics on dielectric substrates," *J. Adhesion Sci. Technol.*, vol. 31, no. 11, pp. 1229–1250, 2017.
[33] K. Zhang and S. Follmer, "Electrostatic adhesive brakes for high spatial resolution refreshable 2.5D tactile shape displays," in *Proc. IEEE Haptics Symp.*, 2018, pp. 319–326.
[34] K. Yatsuzuka, F. Hatakeyama, K. Asano, and S. Aonuma, "Fundamental characteristics of electrostatic wafer chuck with insulating sealant," *IEEE Trans. Industry Appl.*, vol. 36, no. 2, pp. 510–516, Mar./Apr. 2000.
[35] S. B. Diller, S. H. Collins, and C. Majidi, "The effects of electroadhesive clutch design parameters on performance characteristics," *J. Intell. Mater. Syst. Struct.*, vol. 29, no. 19, pp. 3804–3828, 2018.
[36] R. Yeh, S. Hollar, and K. S. Pister, "Single mask, large force, and large displacement electrostatic linear inchworm motors," *J. Microelectromech. Syst.*, vol. 11, no. 4, pp. 330–336, 2002.

Kai Zhang received the B.S. degree from the School of Electronics Engineering and Computer Science, Peking University, Beijing, China, in 2014 and the M.S. degree in electrical engineering in 2016 from Stanford University, Stanford, CA, USA, where he is currently working toward the Ph.D. degree in electrical engineering. His research interests include haptic interfaces for virtual reality and information display, haptic rendering, and human computer interaction. He received the Stanford Graduate Fellowship.

Eric J. Gonzalez received the B.S. degree from the University of Florida, Gainesville, FL, USA, in 2016, and the M.Sc. degree from Stanford University, Stanford, CA, USA, in 2018 with a concentration in Mechatronics. He is currently working toward the Doctoral degree in mechanical engineering with Stanford University. His research interests include the intersection of human computer interaction and haptics. He is a recipient of the Stanford Graduate Fellowship.

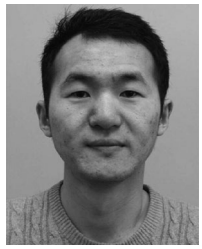

Jianglong Guo is currently a Research Associate with Soft Robotics, Bristol Robotics Laboratory, SoftLab, University of Bristol, Bristol, U.K. His research interests include bio-inspired robotics, controllable adhesion, medical robotics, and soft-smart materials and structures integrated with multimodal sensing, morphologically adaptive actuation, and versatile gripping functionalities.

Sean Follmer is an Assistant Professor of mechanical engineering and computer science (by courtesy) with Stanford University, Stanford, CA, USA. His research interests include human computer interaction, haptics, and human robot interaction that explores the design of novel tactile physical interfaces and novel robotic devices. He directs the Stanford Shape Laboratory and is a faculty member of the Stanford HCI Group.